Journal of Applied Geophysics 159 (2018) 285–293

Contents lists available at ScienceDirect

Journal of Applied Geophysics

journal homepage: www.elsevier.com/locate/jappgeo

2D Synthetic Emitter Array methodology for improving GPR reflections

Darío Bullo, Néstor Bonomo *

IFIBA, CONICET - Departamento de Física, Facultad de Ciencias Exactas y Naturales, Universidad de Buenos Aires - IFIBA, CONICET, Ciudad Universitaria, Buenos Aires 1428, Argentina

ARTICLE INFO

Article history:
Received 20 March 2018
Received in revised form 3 July 2018
Accepted 10 August 2018
Available online 28 August 2018

Keywords:
GPR
Synthetic Emitter Array
Phased Array
Reflection improvement
Clutter
Noise

ABSTRACT

Synthetic 1D-arrays of emitters are used in the area of GPR to improve primary reflections that in single-offset profiles show low continuity and amplitude due to the interference of clutter and noise. In this methodology, at each array position along the survey line, a series of single emitter-receiver measurements is performed, keeping the position of the receiver constant and placing consecutively the emitter at the positions of the nodes of the array grid. A definite phase relation between the traces that constitute each common receiver gather is established and used to shift them in time with respect to the reference-offset trace, and the results are averaged. The phase relations are defined in order to superpose constructively the primary reflections, and reduce the random noise and clutter. The 1D synthetic procedure is equivalent to narrowing the transmitted electromagnetic wave-front along the direction of a real 1D array, which reduces the interference produced by reflectors located in formerly illuminated regions of the soil, and directing the field along an emitters-reflector-receiver path that maximizes the amplitude of the primary reflection at the position of the receiver with respect to the other reflections.

In this article, a previously developed 1D-array method is extended to 2D-arrays, and the results of the 2D extension are analyzed and compared to the results of the 1D-array, Common-Midpoint and Single Offset techniques. The proposed 2D procedure considers a rectangular, homogeneous geometry for the array and a simple phase-relation between the component traces. In addition to directing the wave-front towards the target, these settings make possible to reduce the width of the wave-front along both axes of the array, which is expected to enhance the 1D results. Since the dimensionality increases in the 2D geometry, the number of traces in the summation grows significantly, which should also improve the final result. As a part of the 2D methodology, a variable that represents the reflection improvement, with respect to the Single Offset method, is defined and optimized as a function of the phase differences between adjacent traces along both directions of the array and the position of the emitters-receiver group along the survey line. A final data-section is generated from the optimal values found in this step. To evaluate the results of these methodologies, two basic types of reflections are analyzed: diffractions produced by small objects and reflections at extensive interfaces. Numerical and laboratory data are considered. The effects of different numbers of emitters and distances between them on the results are investigated, in order to obtain the best result. The 2D method shows noticeable enhancements of the continuity and amplitude of the primary reflection with respect to the other methods.

1. Introduction

A single pair of antennae, a transmitter and a receiver, is frequently employed in the investigations carried out with GPR (single pair of elements, SE). The antennae are usually dipolar, and are placed on the soil surface with their long axes parallel to the ground and perpendicular to the line between the dipole centers. Short electromagnetic pulses are transmitted into the soil (time-domain GPR), while the amplitude of the resultant field is measured as a function of time. The antennae are moved along a survey line, often keeping their dipoles perpendicular to it and using a constant distance between the antennae (single offset, SO, or equivalently, constant offset). Then, the amplitude of the electromagnetic field is also registered as a function of the position of the antennae pair. The data are processed and a mean velocity of propagation of the electromagnetic waves in the soil is calculated. The resulting data are represented in vertical or horizontal sections of the soil, from which the main reflectors and layers are finally interpreted. The SE-SO methodology is the most frequent in GPR because, on the one hand, the SO configuration minimizes the acquisition and processing times with respect to variable offset (or, equivalently, multi-offset, MO) configurations (Jol, 2009) and, on the other hand, using SE facilitates acquiring data in areas with appreciable number of obstacles, as rocks, trunks, poles, etc., in which devices that include multiple transmitters and receivers (multi-elements, ME) cannot be easily moved because of their considerably larger size (Bullo et al., 2016; Paglieroni et al.,

* Corresponding author.
E-mail addresses: dbullo@df.uba.ar (D. Bullo), bonomo@df.uba.ar (N. Bonomo).

https://doi.org/10.1016/j.jappgeo.2018.08.005
0926-9851/

2015; Sato et al., 2016). Also as a consequence of this characteristic, SE devices produce better coupling with the soil than ME devices in cases of irregular air-soil surfaces, which is important to optimize the transmission of the fields across this interface and, then, to optimize the results. SE acquisition also minimizes the equipment and transportation costs, despite significantly increasing the fieldwork times with respect to ME acquisition in cases of multi-polarization, MO and dense grid of survey-lines surveys.

In the MO methodologies, each portion of soil is multiply examined by locating the antennae at different positions around it. This increases the amount of information available for determining the investigated characteristics of the soil and enables applying more precise techniques for calculating them. As an example, the number of statistics available for estimating the velocity field grows when these methodologies are applied, and procedures based on coherence calculation can be used to obtain it. Both features improve the velocity estimation and the results of the imaging and positioning of reflectors (Yilmaz, 2001; Forte and Pipan, 2017). Another important benefit of the MO methodologies, with respect to SO, is that they make possible to increase the amplitude ratio of the primary reflections with respect to the other reflections and noise (concisely, signal-to-noise-ratio, SNR), so the former reflections can be better visualized and analyzed. The procedures to filter the clutter and noise are typically based on shifting and stacking the traces of the array so that the primary reflections superpose constructively and the other reflections and noise add destructively.

The Common Midpoint method (CMP) is one of the MO methodologies most frequently used in GPR (Arosio et al., 2016; Martins et al., 2017; Zhao and Al-Qadi, 2016). In the CMP method, a transmitter and a receiver are symmetrically moved from a midpoint, often using a constant increment in the offset. The traces that compose the CMP gather are corrected for the normal move-out and stacked in order to increase the SNR. A small number of midpoints are frequently chosen at positions selected as representative of the studied soil, although denser 1D or 2D grids of midpoints can be defined for more detailed characterizations. With the CMP method, it is possible to obtain precise estimations of the velocity field and to improve the SNR for medium-to-high-depth reflectors and low-to-moderate slopes (Berard and Maillol, 2007; Jacob and Urban, 2016; Yilmaz, 2001).

The Emitter Array (EA) method is a ME technique that employs a set of emitters and a single receiver (Lutz and Perroud, 2006; Liu and Sato, 2014). The array elements emit coordinately, keeping a definite phase relation between them. As a consequence of this characteristic, EAs are a type of Phased Array (Jol, 2009; Kikuchi et al., 2016). The number of transmitters, relative distances and amplitudes are commonly defined in order to reduce the divergence of the resultant field, thus concentrating the energy in a narrower area around the central part of the transmitted wave front. The relative phases between the array components are usually selected with the goal of transmitting the field towards the estimated position of the target. When the transmitters-receiver group is moved across the investigated area, the relative positions and orientations of the antennae with respect to the reflecting surface often vary, so the relative phases between the array components have to be changed in order to redirect the energy along optimum transmitters–reflector–receiver paths. As a consequence of these mechanisms, the SNR and lateral coherence of the primary reflections are improved (Lutz and Perroud, 2006; Cedrina et al., 2010).

The Synthetic Emitter Array (SEA) method is based on synthesizing a field that resembles that of an EA, from a series of single emitter-receiver measurements (Lutz and Perroud, 2006). To obtain the SEA data, SE or ME arrangements can be used. In the first case, a transmitter is successively placed at the positions where the components of the EA would be; in the second case, a set of emitters is used, and the elements emit sequentially. After the data have been acquired, the individual records are corrected in time and stacked to synthesize the field of the array. The EA and SEA methodologies produce similar results, although they are not physically equivalent. In addition to the benefits and limitations of the SE techniques, the SE version of the SEA methodology makes possible selecting arbitrarily the distance between the array components, so distances smaller than the size of the elements can be used if necessary, and minimizes coupling between the antennae (Sato and Takayama, 2009). It also avoids selecting the relative phase before acquiring the data, as occurs with EAs.

A SEA methodology that employs 1D-arrays has been investigated by the authors of the present work in the past (Cedrina et al., 2010, 2011). This methodology has proved to be suitable for improving low-quality reflections, for diverse types of reflections and characteristics of their environment. Significant improvements of the SNR and continuity of the primary reflections have been obtained by using this methodology, with respect to SO and CMP. Taking these capabilities into account, it seems interesting to extend the 1D methodology to 2D arrays. 2D arrays can reduce the width of the synthesized main lobe along both horizontal directions of the array and increase the number of statistics, which are expected to enhance the 1D-SEA results, without increasing significantly the length of the array and distorting the shape of the central part of the wave-front as a consequence of the larger differences between the propagation distances of the component waves (Cedrina et al., 2011).

In this work, we extend our previous 1D-SEA methodology to 2D arrays, and examine the ability of a 2D procedure to improve primary reflections with respect to the surrounding clutter and noise. After describing the methodology (next section), we evaluate its results by applying it to the diffraction produced by a small object and the reflection at an extensive interface. These types of reflections are typical of the GPR data sections. Numerically simulated and laboratory data are analyzed. The results of the 2D-SEA, 1D-SEA, CMP and SO methodologies are compared. The performance of the methods is evaluated as a function of the number of dipoles, distances and relative phases between the array components.

2. Methodology

The proposed methodology is explained in this section as it is applied to a simulated example. Fig. 1a shows a rectangular array composed of N_x x $N_y = 5 \times 5$ emitting dipoles, E_i^j, $0 \le i \le N_x\text{-}1$, $-(N_y\text{-}1)/2 \le j \le (N_y\text{-}1)/2$. The dipoles are spaced at regular intervals $d_x = d_y = 0.05$ m, in the $\hat{x}$ and $\hat{y}$ directions, respectively. Since the array geometry is 2D, we use this nomenclature to refer to the array and the associated methodology, even though the latter is applied to 3D datasets, as will be explained in the next paragraphs. A receiving dipole, R, is located at a distance $h = 0.20$ m from the nearest emitter in the array, E_0^0. This emitter is set as a reference for the array. The relative positions of the other emitters with respect to it are $\vec{r}_i^{\,j} - \vec{r}_0^{\,0} = (-idx, jdy, 0)$, in x-y-z coordinates. All the dipoles are oriented along the y axis. A spherical cavity with radius $r_s = 0.03$ m, electric permittivity relative to vacuum $\varepsilon_p = 1$, magnetic permeability relative to vacuum $\mu_p = 1$ and conductivity $\sigma_p = 0$ mS/m was located at the position (2.40, 0, 0.75) m. This cavity

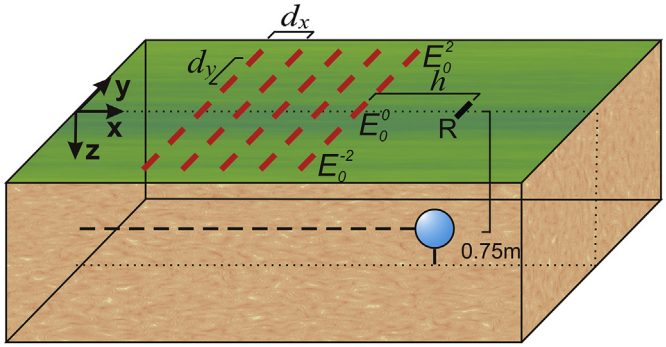

Fig. 1. 2D array geometry and small reflector configuration.

will produce a diffraction signal in the data sections due to its small size with respect to the wavelength of the electromagnetic waves in the surrounding medium ($\lambda_m = 0.3$ m, for a velocity of propagation $v =$ 0.15 m/ns and a frequency $f_0 = 500$ MHz). In this medium, the electromagnetic parameters are $\varepsilon_m = 4, \mu_m = 1$ and $\sigma_m = 0.1$ mS/m. Several secondary small-size reflectors are included in the model in order to add clutter to the resultant data sections. Their electromagnetic parameters vary in the intervals $\varepsilon_s = [3.4–4.6]$ and $\sigma_s = [0.9–1.1]$ mS/m, while $\mu_s = 1$.

In a ME array, all the elements shown in Fig. 1 emit simultaneously or sequentially as the amplitude of the electric field is measured at the position of *R*. In a SE array, only one emitter is used and successively placed at the positions of the array, and a trace is registered for each of these positions. This is the option considered in this work. Once the set of N_x x N_y traces has been obtained at a position of the SEA-receiver group, the whole group is moved a constant distance Δx along the x axis, and the procedure is repeated. In the simulations of this section, $\Delta x = 0.05$ m, and a Ricker-type of wave-packet is used for the emitting dipole. The central frequency of the transmitted pulse is $f_0 = 500$ MHz. We employed the GPRMax finite-differences code (Giannopoulos, 2005) to simulate the data. The size of the grid was 4.8 m × 1.6 m × 1.7 m, in the x-y-z directions, respectively, and the size of the grid elements was 0.01 m × 0.01 m × 0.01 m.

A series of common-receiver gathers is obtained along the survey line through the described procedure. To synthesize the field of the array at each position of the group, a time shift dt_i^j with respect to the reference trace is applied to each component trace. To define dt_i^j, constant increments between neighboring traces, dt_x and dt_y, are assumed along the *x* and *y* directions, respectively, and a reflection symmetry with respect to $\hat{x}$ is adopted. The mathematical expression for the time shift is the following:

$$dt_i^j = -i dt_x - |j| dt_y \tag{1}$$

Once the traces have been shifted in time, the resultant traces are averaged using constant relative amplitude factors $A_i^j = 1$ in the summation. A_i^j is a real quantity that multiplies the amplitude of the trace *i,j*; then, selecting $A_i^j = 1$ for all *i, j* implies that the traces have the same weight in the summation. As the emitters and the receiver are orthogonal to the survey line, the stacking is performed on traces that represent the same component of the field (*y* polarization).

As a consequence of the previous criteria, the direction of the main lobe of the resultant field in the *x-z* plane is controlled by the parameter dt_x, and the *y*-width of the field is controlled by dt_y. In this way, these relevant characteristics of the synthesized field depend on single parameters, which can take continuous values, have no range limitations, and do not require changing the array geometry when modified. This considerably simplifies the simulation or acquisition of data, the subsequent optimization procedure and the interpretation of results. On the other hand, the investigations carried out for 1D arrays have demonstrated that the *x*-width of the wave front plays a secondary roll in the reflection improvement, compared to directing the wave front towards the target (Cedrina et al., 2011). In the proposed method, the *x*-width is controlled through d_x and N_x, which are varied in discrete steps in order to evaluate their effects on the final results.

The next step in the 2D-SEA methodology is to determine values of dt_x and dt_y that optimize the primary reflection along the survey line; these values are named dt_x^* and dt_y^*, respectively. A combination of three variables is used to quantify the quality of the primary reflection (Cedrina et al., 2011): 1) the correlation between nearby traces, calculated along a time window that fits approximately the main reflection (*Cor*), 2) the time difference of the peak amplitude of neighboring traces (Δt) and 3) the quotient of the average amplitudes of the primary reflection and the signals around it (*SNR*), calculated along the time window mentioned above and a similar window defined for the surrounding signals, respectively. In the presence of clutter and noise, these variables are expected to deviate from the ideal values, 1, 0 and ∞, respectively. The magnitudes of the deviations increase when the quality of the result decreases. To simplify the optimization process, the three variables are combined into a single global one:

$$Glb = Cor * SNR/\Delta t \tag{2}$$

and, finally, the SEA and SO results are compared:

$$NGlb = Glb^{SEA}/Glb^{SO} \tag{3}$$

From this definition, *NGlb* is >1 if the SEA result is better than the SO result and <1 otherwise.

Fig. 2 shows *NGlb* as a function of dt_x, dt_y and the position of the midpoint between *R* and $E_{0,0}$, x_a. In Fig. 2a, a cutoff value $NGlb^0 = 3$ has been used in order to display the subset of data that produces the highest values of *NGlb*. The resultant data volume is narrower along the coordinate dt_x than along the coordinate dt_y. This implies that choosing optimal values of dt_x requires more attention than choosing optimal values of dt_y. Nevertheless, selecting these values with high precision is not crucial, since the volume presents non negligible widths in both directions, which is a positive characteristic of the methodology.

Fig. 2b and c shows slices of *NGlb* along surfaces that include the optimal curve. The surfaces are defined as $dt_y = dt_y^*(x_a)$ and $dt_x = dt_x^*(x_a)$, respectively. The intersection of these surfaces agrees with the optimal curve, which is indicated with a full line in the figures. It has been obtained by fitting a smooth curve to the data within the volume of Fig. 2a. The central position of the volume changes visibly in the coordinate dt_x as the array is moved along x_a. This characteristic manifests the importance of selecting different values of dt_x along the survey line in order to direct adequately the wave-front towards the target. On the other hand, the volume presents a considerably larger width in the coordinate dt_y, which is approximately constant along x_a. This indicates a

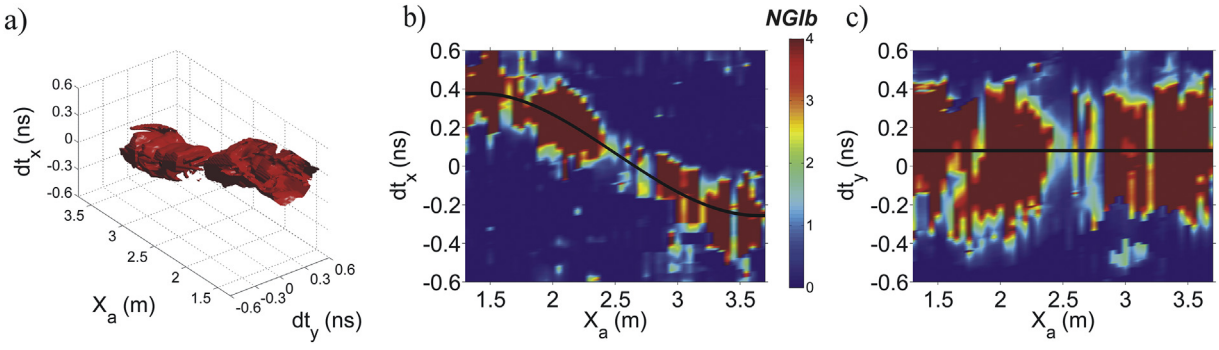

Fig. 2. *NGlb* as a function of dt_x, dt_y and x_a, for the model of Fig. 1. a) Data subset with *NGlb* > 3. b) and c), slices of *NGlb* along the optimal curve, for $dt_y = dt_y^*(x_a)$ and $dt_x = dt_x^*(x_a)$, respectively. The optimal curve is indicated with a full line.

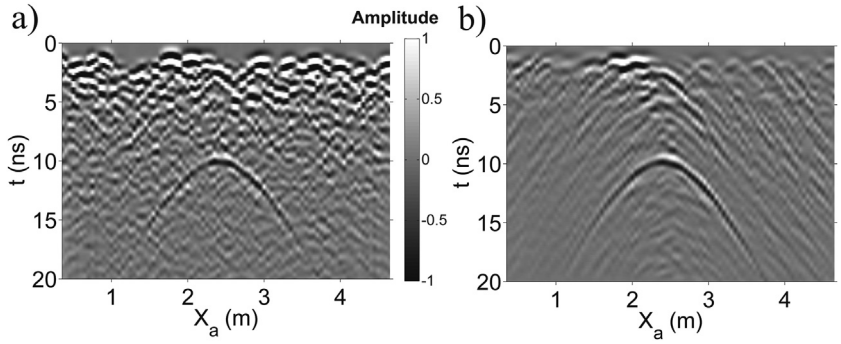

Fig. 3. a) SO and b) optimal 2D-SEA profiles obtained for the example of Fig. 1.

lower sensitivity of *NGlb* to variations of dt_y. This sensitivity can be improved by increasing N_y or dy in the array settings.

Fig. 3 shows the a) SO and b) optimal 2D-SEA profiles obtained for the example of this section. The offset in the SO configuration of Fig. 3a is $h = 0.20$ m, as well as the distance between E_0^0 and R in Fig. 3b. The trace interval is $\Delta x = 0.05$ m in both figures. From the comparison of these figures, the improvement in the SNR and continuity of the main reflection is clear. The average values of *NCor*, $N(1/\Delta t)$, *NSNR* and *NGlb* are 1.7, 3.4, 2.6 and 8.1 respectively, which indicate improvements in the four variables. These variables are defined as $NCor = Cor^{SEA}/Cor^{SO}$, $N(1/\Delta t) = N(1/\Delta t)^{SEA}/N(1/\Delta t)^{SO}$, and $NSNR = SNR^{SEA}/SNR^{so}$.

Before finishing this section, it is worth mentioning that the main characteristics of the 2D-SEA results described in the previous paragraphs have been verified for different parameters of the array, diffractor and soil. In the case of extensive reflectors, these characteristics are qualitatively similar to those of the analyzed example, provided that the survey line is oriented along the dip direction (dt_x^* is less sensitive to x_a in the case of extensive reflectors than in the case of diffractors).

Optimizing the results of a trace-stacking as a function of the array parameters in a real situation can be a difficult task if the characteristics of the soil are significantly variable or insufficiently known. For example, the primary reflectors can occupy near to far-field regions of the soil, and the velocity field and topography can have important fluctuations and be sparsely known. Theoretical approximations and empirical approaches can be useful in these situations, but they are not general. Then, it is relevant that the simple methodology described in this section and, in general, the SEA methodologies are useful regardless of these factors, and that they usually lead to satisfactory results.

3. Results

The 2D-SEA method is applied in this section to laboratory data, and the results are analyzed and compared to the results of the 1D-SEA, CMP and SO methods.

3.1. Diffraction produced by a small reflector

In the first experience, a setup similar to that of Fig. 1 was used. An expanded-polystyrene sphere with radius $r_s = 0.03$ m was coated with a 0.2 mm-thick aluminum foil and located in a 1.5 m × 0.8 m × 0.6 m box, filled with sand up to a height of 0.5 m (Fig. 4a). The position of the sphere was $\vec{r}_s = (0.75, 0, 0.20)$ m. A total of 10 metallic nails, screws and rivets were dispersed in the sand volume in order to generate clutter. The propagation velocity in this medium was $v = 0.17 \pm 0.01$ m/ns.

A square geometry, with $N = N_x = N_y = 7$, was used to acquire the data. This made possible to construct three square synthetic arrays ($N = 3, 5, 7$) with the characteristics described in the previous section, by selecting subsets of the measured traces. The parameter $d = d_x = d_y$ varied in the interval 0.01–0.05 m, with increment $\Delta d = 0.01$ m. Five datasets, each for a different value of d, were acquired along the survey line. With these settings, a total of 15 SEA arrays could be constructed, which were determined by the different combinations of d and N. The distance between E_0^0 and R was $h = 0.14$ m, the minimum value compatible with the sizes of the antennae, and $\Delta x = 0.01$ m. The dipoles of the antennae were aligned with $\hat{y}$, and the survey line agreed with $\hat{x}$. A pulseEKKO PRO unit (Sensors and Software Inc.) was used, and the nominal central frequency of the antennae was $f_0 = 1$ GHz.

The data were preprocessed by using dewow, time zero correction and removal of the direct-waves. The 2D-SEA methodology was then applied to the data. The SO and optimal 2D-SEA profiles, for $N = 7$ and $d = 0.03$ m, are shown in Fig. 5a and b, respectively. In the SO profile the offset is $h = 0.14$ m, and the trace interval is $\Delta x = 0.01$ m. Figs. 5c–e show the results of the 1Dx-SEA, 1Dy-SEA and CMP methods, respectively. The 1Dx-SEA and 1Dy-SEA geometries were defined from the original 2D geometry, as the central row (x direction) and the column closest to R (y direction) of the matrix, respectively, so the element E_0^0 was part of both 1D arrays. A 1D version of the optimization procedure described in the previous section was used in these cases. In the CMP methodology, the antennae were positioned along the x axis, with their dipoles parallel to $\hat{y}$. In the minimum-offset configuration, the positions of the emitter and receiver agreed with the positions of E_0^0 and R in the SEA arrays. Since the CMP geometry was only partially included in the SEA-2D geometry, the CMP data were acquired separately. This procedure was less laborious and complicated than increasing the size of the SEA array and extracting the CMP traces from it. After

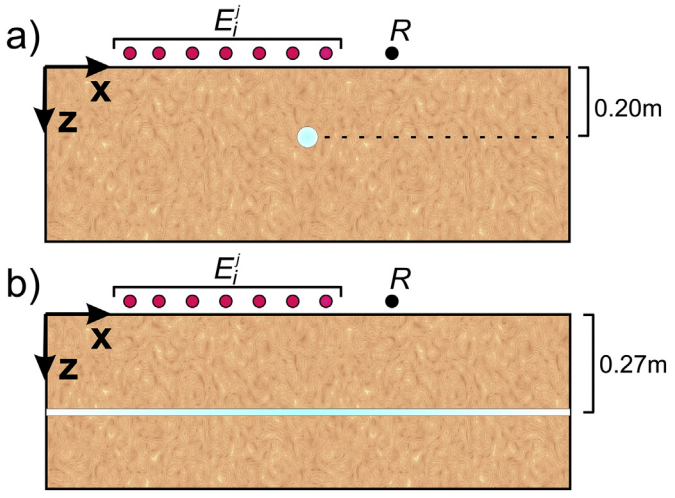

Fig. 4. Schemes of the soil models used in the experimental examples. a) Small reflector, b) extensive horizontal reflector.

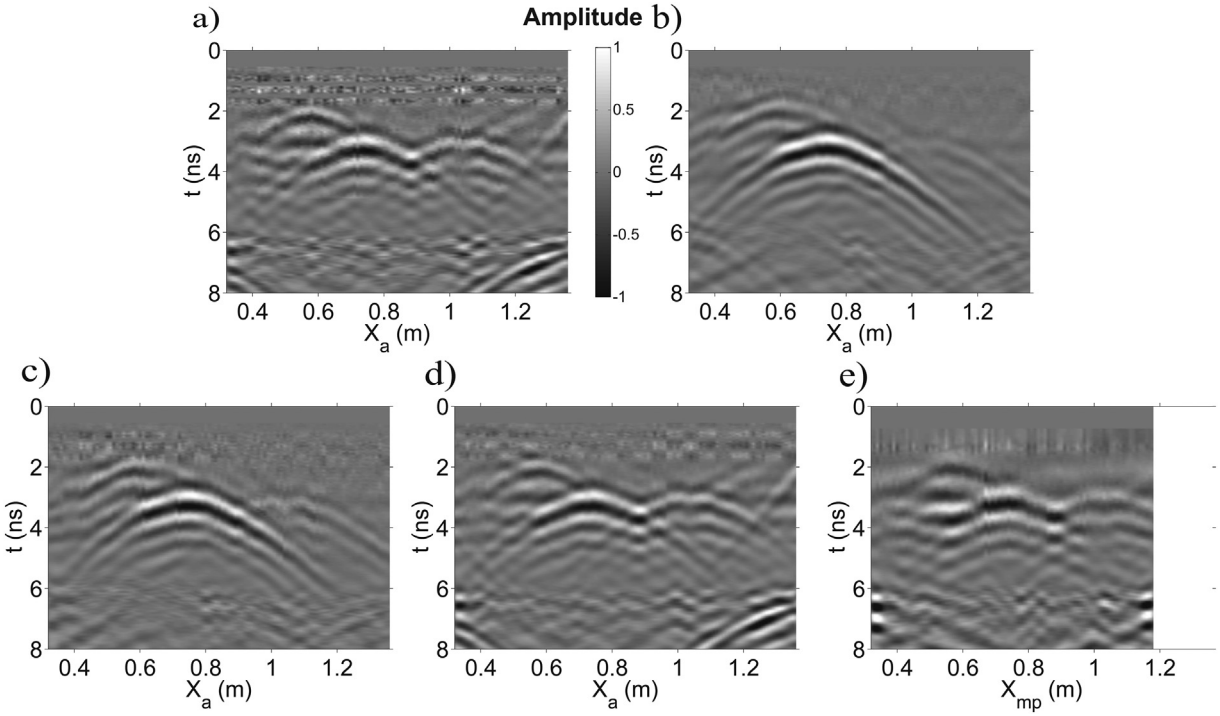

Fig. 5. Results of applying the investigated methodologies to the diffraction produced by a small object. a) SO, b) 2D-SEA, c) 1Dx-SEA, d) 1Dy-SEA and e) CMP data sections.

the preprocessing steps mentioned above, the CMP data were move-out corrected and stacked, and finally represented in a data section, as shown in Fig. 5e. In this procedure, the stacking velocity was approximated by the velocity of propagation, since it was almost constant throughout the container. In cases with more complex soil models that include horizontal layers and velocity variations, semblance analysis can be performed instead. The offset range in the Fig. 5e is off= [0.14 0.50] m, and the increment Δoff= 0.06 m ($N = 7$, $\Delta off = 2^{*}d$). The horizontal coordinate, x_{mp}, corresponds to the position of the midpoint. The x_{mp}-range is shorter than the x_a-ranges of the previous figures because, in the CMP configuration, R found the end of the sand box before it did in the SEA configurations.

The discussion of the results of Fig. 5 starts with the methodology that produces the lowest improvement. Fig. 5e shows that the CMP method has reduced part of the clutter present in the original SO profile (Fig. 5a). A higher SNR is observed for x_{mp} near the position of the vertex of the diffraction hyperbola, $x_{mp}\approx 0.75$ m, $t\approx 2.5$ ns, than towards its asymptotes. This occurs because the CMP method is originally designed to improve the signals of approximately horizontal reflectors located below the midpoint, and not the signals of small reflectors that are laterally displaced with respect to it. Also for this reason, the continuity of the reflection increasingly deteriorates as x_{mp} moves away from the position of the vertex of the hyperbola. Fig. 5d shows that the 1Dy method has also removed part of the clutter of the SO section. This is a consequence of decreasing the size of the synthesized wave front along the y coordinate. In this way the secondary diffractors located in the peripheral part of the lobe become less illuminated and their clutter effects diminish. In contrast to the CMP method, the 1Dy-SEA result shows both continuity and SNR improvement along the entire x_a range, which is a positive characteristic of the methodology. Regarding the 1Dx result, Fig. 5b, it is clear that the continuity and SNR of the main reflection have been significantly improved with respect to the previous cases, as a consequence of directing the resultant wave-front towards the main diffractor, as well as reducing the size of the wave-front along $\hat{x}$. In this case, the improvement is important towards the asymptotes of the hyperbola; in particular, the diffraction with vertex at $x_a\approx 1.03$ m, $t\approx 2.6$ ns and the diffractions originated at the borders of the container have been appreciably attenuated. On the contrary, the reflection with vertex at $x_a\approx 0.62$ m, $t\approx 1.5$ ns has almost not been affected by the 1Dx procedure, due to the proximity of the correspondent reflector and the main diffractor. Finally, it is clear that the 2D-SEA method, Fig. 5b, has produced the best result among the evaluated methods. The main reasons for this are that the 2D methodology takes advantage of all the aforementioned mechanisms and, in addition, significantly increases the number of averaged terms. In particular, the jiggle visible in the 1Dx data section at $x_a\approx$ 0.61 m, 0.72 m, 0.85 m, etc., and the interference effect of the diffraction with vertex at $x_a\approx 1.03$ m, $t\approx 2.6$ ns almost disappeared in the 2D section. As a consequence of the 2D improvements, the main reflection can be observed for a larger range of x_a.

In Fig. 6, the parameters N and d of the 2D array have changed with respect to Fig. 5b. In Fig. 6a, $N = 3$, i.e., a number of dipoles below the previous one (distance between dipoles $d = 0.03$ m). It is clear that the quality of the main reflection deteriorates with this modification, which occurs as a consequence of augmenting the width of the wave front and diminishing the number of averaged traces. In Fig. 6b and c, the distance between the dipoles is $d = 0.01$ m and $d = 0.05$ m, which are below and above the value used in Fig. 5b, respectively (number of dipoles $N = 7$). A comparison of the three figures shows that the 2D-SEA result gets worse for $d = 0.01$ m, as the array of emitters tends to resemble a single source and the size of the wave front increases. For $d = 0.05$ m, the result is quite similar to that obtained for $d = 0.03$ m, which seems to indicate that the signal improvement is optimum around these values of d.

Fig. 7a shows the average value of $NGlb^{*}$, $\langle NGlb^{*}\rangle$, calculated throughout the entire x_a interval, as a function of d. Here, the asterisk indicate that $NGlb$ is evaluated at (dt^{*}_{x}, dt^{*}_{y}). The curves correspond to the three SEA methodologies and the three values of N considered in this section. To reduce the fluctuations in the curves, the highest 10% of the values of $NGlb^{*}$ have been excluded from the average. All the curves in the figure show improvement with respect to the SO result ($\langle NGlb^{*}\rangle > 1$). For a fixed value of N, the 2D curves exceed clearly the 1Dx curves, which in turn exceed the 1Dy ones. The quotients of the $\langle NGlb^{*}\rangle$ values obtained from the different methods, averaged along the curves, are 1.7 and 2.1,

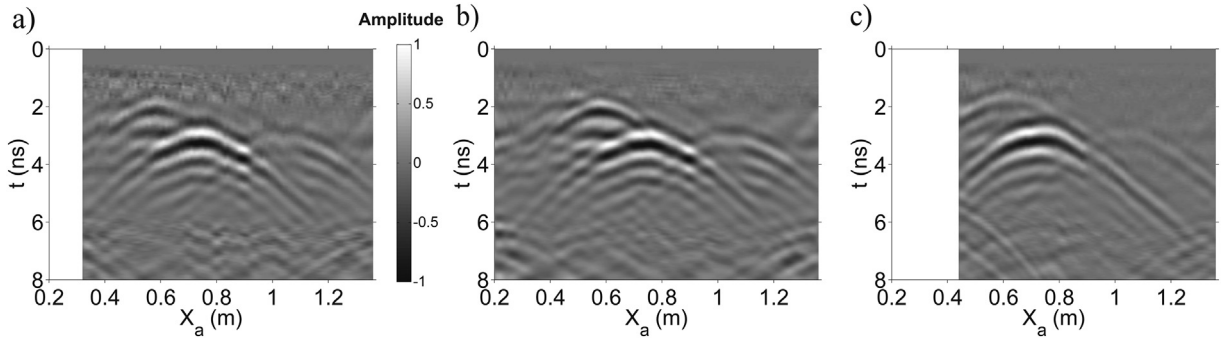

Fig. 6. 2D-SEA data sections for, a) $N = 3$, $d = 0.03$ cm, b) $N = 7$, $d = 0.01$ cm and c) $N = 7$, $d = 0.05$ cm. The data sections correspond to the small reflector experience.

for 2D/1Dx and 1Dx/1Dy, respectively. For a fixed value of d, $\langle NGlb^* \rangle$ increases with N. As an example of this behaviour, Fig. 7b shows $\langle NGlb^* \rangle$ as a function N, for $d = 0.03$ m. The CMP results have been also included in this figure for comparison. Among all the methods, CMP has produced the lowest improvement, which is slightly below the one produced by the 1Dy-SEA method. The values of $\langle NGlb^* \rangle > 1$ obtained for the CMP method seems to contradict what was expressed from the direct inspection of the radargrams (Fig. 5a and e), that is, that most of the CMP reflection deteriorated with respect to the original SO reflection. Nevertheless, this result is explained by the relatively large values of SNR obtained around the vertex of the hyperbola, which compensates the low values of $\langle NGlb^* \rangle$ obtained for the other parts of it and produces an overall result slightly grater than 1. Fig. 7b also illustrates that the 1Dx-SEA and 2D-SEA curves monotonically increase with N, that the 1Dx-SEA results are much better than the results of the CMP and 1Dy-SEA methods, and that the 2D-SEA method produces the best results.

3.2. Reflection at an extensive interface

The second example analyzed in this section corresponds to the reflection at a horizontal slab (Fig. 4b). The slab was composed of a gypsum material and had a thickness of $\Delta z_s = 0.01$ m. It was buried in the sand box at a depth $z_s = 0.27$ m and it occupied the whole x-y area of the box (same coordinate system that in the previous examples). 10 metallic nails and rivets were located throughout the sand volume. The GPR and array parameters used in this case were similar to those of the previous experience.

Fig. 8 shows the data sections obtained by applying the: a) SO, b) 2D-SEA, c) 1Dx-SEA, d) 1Dy-SEA and e) CMP methods. As in the previous experience, the analysis begins with the last figure (Fig. 8e). This figure shows that the CMP method has attenuated the interference effects of the most intense secondary reflections, that is, the diffractions with vertexes at $x_{mp} \approx 0.38$ m, $t \approx 1.8$ ns and $x_{mp} \approx 1.30$ m, $t \approx 1.9$ ns. Nevertheless, some discontinuities are still visible along the primary reflection, for example, at $x_{mp} \approx 0.56$ m, 0.68 m, 0.86 m and 1.05 m. The CMP method has also improved the amplitude of the main reflection with respect to other approximately horizontal signals around it, as a remnant of the direct waves, which occurs for $1.8 < t < 3.2$ ns, and later oscillations of the primary reflection, which are visible for $4.6 < t < 5.5$ ns, approximately. The direct waves are attenuated since their signals are destructively superposed during the stacking, because they propagate with a velocity larger than the stacking velocity (which is approximately the velocity of propagation in the sand). The later oscillations tend to be removed since their amplitudes become negligible for large offsets, and the stacked amplitude diminishes when these negligible terms are included in the summation. The 1Dy-SEA result (Fig. 8d) shows some improvement with respect to SO, in particular, in the continuity of the central part of the main reflection. The origin of this improvement is the same that was mentioned in the previous experience. The prominent diffraction tails that interfere with the main reflection and the surrounding horizontal signals are not as attenuated in this case as in the CMP case, so the 1Dy-SEA method presents an overall result inferior to CMP. The 1Dx-SEA method (Fig. 8c) has led to a data section with similar characteristics than the CMP method, although with a better continuity and SNR of the main reflection. The best result is obtained for the 2D-SEA method (Fig. 8b), which has further reduced the intensity of the diffractions around the primary reflection and almost completely removed the discontinuities.

Fig. 9 shows the 2D-SEA results obtained using arrays with a) $N = 3$, $d = 0.03$ m b) $N = 7$, $d = 0.01$ m and c) $N = 7$, $d = 0.05$ m. The other array parameters are the same that in the previous figure. As occurred in the small reflector experience, the improvement obtained for the horizontal reflection diminishes as $N \to 1$ and $d \to 0$, whereas it remains almost unchanged when d is increased from 0.03 m to 0.05 m.

Fig. 10 shows $\langle NGlb^* \rangle$ as a function of a) d, for the considered SEA methods and N as a parameter, and b) N, for all the analyzed methods and $d = 0.03$ m. These figures are analogous to Figs. 7a-b of the small

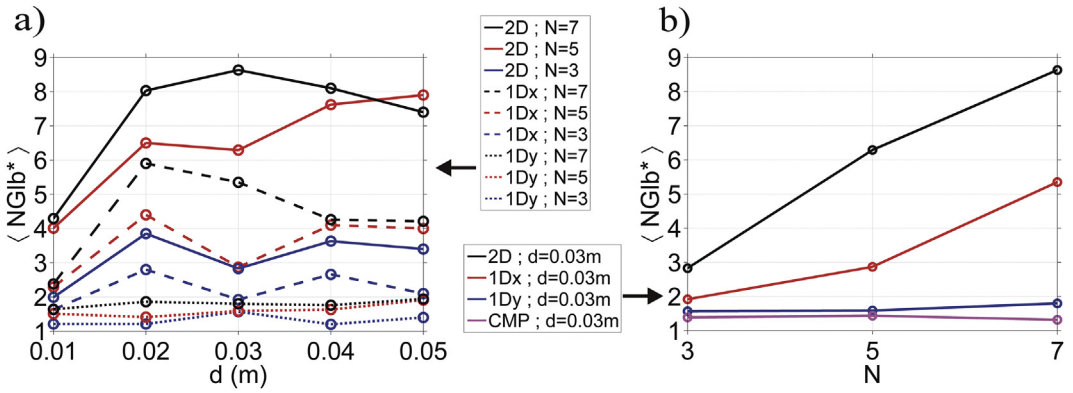

Fig. 7. $\langle NGlb^* \rangle$ as a function of a) d, b) N, for $d = 0.03$ m. The curves correspond to the small reflector experience.

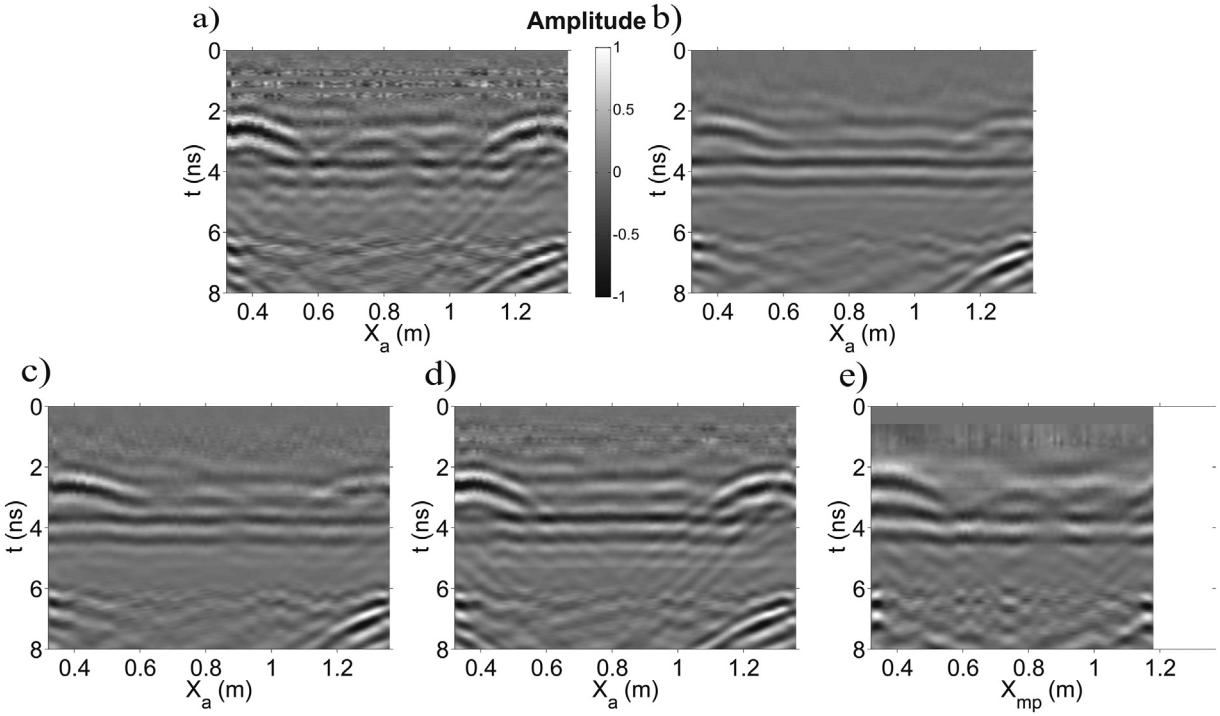

Fig. 8. a) SO, b) 2D-SEA, c) 1Dx-SEA, d) 1Dy-SEA and e) CMP data sections obtained in the extensive reflector experience.

reflector experience. It can be observed from Fig. 10a that the 1Dx-SEA method has enhanced the 1Dy-SEA results, and that the largest improvement has been produced by the 2D-SEA procedure. The average $\langle NGlb^{*}\rangle$ quotients are 1.8 and 1.6, for 2D/1Dx and 1Dx/1Dy, respectively. For fixed values of N, the improvement increases as d changes from 0.01 m to 0.02 m, and it is approximately constant for larger values of d. For fixed values of d, the improvement increases with N (Fig. 10b). When the CMP curve is compared to the SEA ones, it is noted that the former method has produced better results than the 1Dy-SEA method and similar results to the 1Dx-SEA one. The relatively good performance of the CMP method in this experience is a consequence of the aforementioned ability of the method to improve horizontal reflections. The better performance of the CMP method for extensive reflectors than for diffractors can be also confirmed from a comparison of Figs. 7 and 10.

It is expected that $\langle NGlb^{*}\rangle$ decreases for values of N and d beyond those of Figs. 7 and 10. A first reason for this is that the amplitude of the reflections in the data sections becomes negligible for large enough distances between the antennae, due to the different processes of wave attenuation, and adding such negligible terms to the average summation reduces the amplitude of the final result. This effect is, in relative terms, more important for the primary reflections than for the clutter. On the other hand, the amplitude of the noise tends to stabilize for those values of N and d. As a final result, the SNR decreases. The other reason for expecting this behaviour is that, for large values of N and d, the time shifts necessary to put all the traces in phase at the position of the receiver are no longer approximately constant, so eq. 1 becomes increasingly inexact and the traces do not superpose optimally. Unfortunately, the decreasing behaviour of $\langle NGlb^{*}\rangle$ for large values of N and d could not be experimentally confirmed from the implemented setup, mainly due to the relatively small size of the available container. In spite of this, the tendency was confirmed from simulated experiences, for different reflectors and soil models (results not shown).

4. Discussion and conclusions

A 1D-SEA methodology has been extended to 2D-arrays. A rectangular, homogeneous grid of emitters was considered. For practical reasons, this is one of the geometries that can be most easily implemented in a laboratory or in the field. A relation between the time-zero of the component traces and the array parameters was established. It was defined with the main objectives of controlling the propagation direction and transversal width of the synthesized wave front through independent, continuous parameters, which had not range limitations and didn't require modifying the array geometry when they vary. This considerably

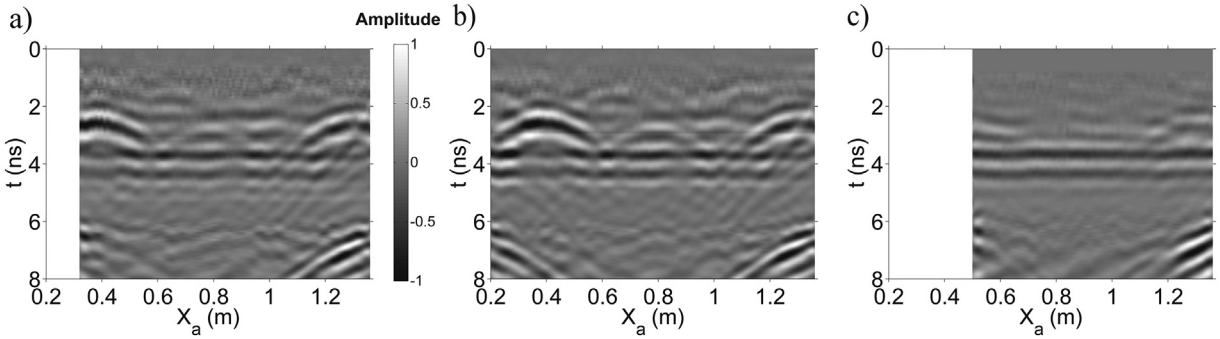

Fig. 9. 2D-SEA data sections for, a) $N = 3$, $d = 0.03$ cm, b) $N = 7$, $d = 0.01$ cm and c) $N = 7$, $d = 0.05$ cm. The data sections correspond to the extensive reflector experience.

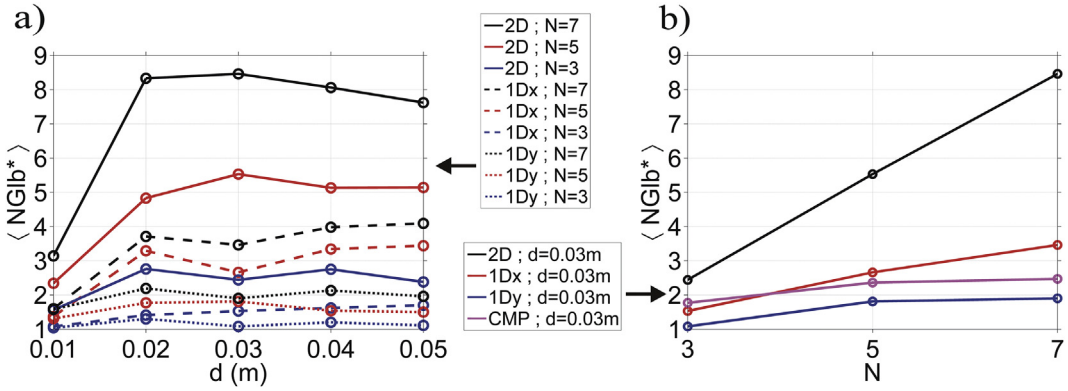

Fig. 10. $\langle NGlb^* \rangle$ as a function of a) d, b) N, for $d = 0.03$ m. The curves correspond to the extensive reflector experience.

simplifies the acquisition of data, the subsequent optimization procedure and its interpretation. The parameters were the time shifts between adjacent traces, defined along the two main axes of the array. Both shifts were assumed constant and symmetric with respect to the survey line throughout the array, for each position of the emitters-receptor group. The width of the wave front along the survey line, which is a secondary factor in comparison to the wave front orientation, was controlled through the number of dipoles and distances between them. These parameters varied discretely and through limited ranges, mainly due the nature of N, the large times required for acquiring data for different array geometries, and the small size of the available container.

The improvements in the continuity and SNR of the primary reflections were quantified through a global variable, which was optimized as a function of the time shifts and the position of the emitters-receiver group. An optimal curve was obtained by fitting a smooth curve to the data with largest values of signal improvement. Since the improvement was quite fluctuating with these variables, producing an appreciable amount of statistics from using small increments in the time shifts was important to achieve a reliable result. A final SEA profile was obtained from the set of variables that generated the optimal reflection improvement.

To evaluate the results of the analyzed methodologies, two characteristic types of reflections were considered: diffractions at small objects and reflections at extensive interfaces. Experimental data were acquired for a sphere located below the survey line and a horizontal slab, respectively. The main characteristics of the 2D-SEA, 1Dy-SEA, 1Dx-SEA, CMP and SO profiles were qualitatively analyzed, and the relative magnitudes of the signal improvement produced by the methods with respect to SO were compared. The 1Dy-SEA method led to a relatively small improvement of the primary reflection, from reducing the width of the synthesized wave front in the direction perpendicular to the survey line. The 1Dx methodology generated a considerably larger improvement than the 1Dy methodology, from directing the wave front towards the reflector and reducing the width of the wave-front in the direction of the survey line. In the small reflector case, the results of the CMP method were similar to the results of the 1Dy-SEA method, whereas in the extensive reflector case, the CMP results were similar to the 1Dx-SEA ones. The better performance of the CMP method in the second experience is a consequence of its capability to improve extensive reflections, but not diffractions. On the contrary, the SEA methods led to more similar outcomes in both experiences. Finally, the 2D-SEA method clearly outperformed the previous methods from reducing the wave-front width in both horizontal directions, orienting the wave front towards the target and increasing significantly the number of terms in the trace summation.

It was observed that selecting correctly both time shifts along the survey line is relevant to optimize the primary reflections through the 2D-SEA methodology. Nevertheless, selecting the time shifts with high precision is unnecessary, since the results are not significantly modified by moderate variations of these parameters. Then, the 2D procedure can be flexibly implemented in practical situations. An adequate choice of the number of emitters and distance between them is also important to obtain satisfactory results. The reflection improvement increased with N, for the values of N considered in the experiences ($N = 3, 5, 7$). On the other hand, the improvement initially increased with d ($d \in [1–2]$ cm) and then remained approximately constant ($d \in [2–5]$ cm). For larger values of N and d, it is expected that the improvement decrease. Similar results to those mentioned in these paragraphs have been obtained from simulated data, and different parameters of the reflectors, clutter and noise.

The SEA methodologies are usually applied to improve reflections that have been qualified as relevant from previous analyses of SO sections. This is so because acquiring SEA data is much more time consuming than acquiring SO data. In this regard, analyzing numerically simulated SEA-responses before acquiring the data can be useful to limit the ranges of N and d that will be considered in the fieldworks and, then, to reduce the acquisition time. The input data to the SEA method do not require more processing steps than the SO method, typically, time-zero correction, dewow, removal of the direct signals and application of gain. Furthermore, this method does not need information about the velocity field, topography and depth of the reflectors, and works for near to far field conditions and variable velocities. To these characteristics, the 2D-version of the SEA methodology adds a significantly larger signal improvement than the previous 1D versions. Future work is planned to investigate the results of employing alternative geometries for the 2D array, with the goal of further improving the characteristics of the synthesized wave front. Other topics that seem worth to be studied are using alternative phase relations between the components of the array in order to optimize the results for large number of emitters and distances between them, and to investigate modifying the relative amplitudes between the components in order to compensate for amplitude differences due to the individual ray paths.

Although the 2D-SEA methodology has been studied in this article in relation to reflectors with basic geometries, it is also applicable to more general reflectors, as interfaces with variable slopes and orientations. Since the SEA methodologies improve discontinuous and low amplitude reflections, they are useful for tracking them across the data sections (Cedrina et al., 2011) and for improving the accuracy of different calculations (Bullo et al., 2016). These characteristics are important in relation to many applications. For example, in Sedimentology, floodplains and areas of fluvial-aeolian interaction can show complex 3D systems of reflections with apparent discontinuities and low response levels due to very variable soil conditions and significant moisture content; in Archeology, discontinuous and low SNR reflections are usual due to deterioration of the structures by natural and cultural agents. In these cases, the 2D-SEA method can help to resolve the buried structures

and increase the precision of the velocity field, so an improved interpretation of the soil can be obtained.

Acknowledgements

This work was partially supported by CONICET and ANPCYT.

References

Arosio, D., Deparis, J., Zanzi, L., Garambois, S., 2016. Fracture characterization with GPR: A comparative study. Proceedings of the16th International Conference of Ground Penetrating Radar, p. 7572679.

Berard, B., Maillol, J., 2007. Multi-offset ground penetrating radar data for improved imaging in areas of lateral complexity – applications at a Native American site. J. Appl. Geophys. 62, 167–177.

Bullo, D., Villela, A., Bonomo, N., 2016. Azimuth calculation for buried pipelines using a synthetic array of emitters, a single survey line and scattering matrix formalism. J. Appl. Geophys. 134, 253–266.

Cedrina, L., Bonomo, N., Osella, A., 2010. An application of the Synthetic Emitter-Array method to improve GPR signals. J. Appl. Geophys. 70, 237–244.

Cedrina, L., Bonomo, N., Osella, A., 2011. GPR-signal improvement using a synthetic emitter array. J. Appl. Geophys. 74, 123–130.

Forte, E., Pipan, M., 2017. Review of multi-offset GPR applications: data acquisition, processing and analysis. Signal Process. 132, 210–220.

Giannopoulos, A., 2005. Modelling ground penetrating radar by GprMax. Constr. Build. Mater. 19, 755–762.

Jacob, R., Urban, T., 2016. Ground-Penetrating Radar velocity determination and precision estimates using Common-Midpoint (CMP) collection with hand- picking, semblance analysis and cross-correlation analysis: a case study and tutorial for archaeologists. Archaeometry 58, 987–1002.

Jol, H., 2009. Ground Penetrating Radar. Theory and Applications. Elsevier, Amsterdam, p. 524.

Kikuchi, K., Mikada, H., Takekawa, J., 2016. Applicability of Phased Array Antenna to Ground Penetrating Radar for Subsurface Imaging Below Surface Obstacles. 78 EAGE Conference and Exhibition: Efficient Use of Technology – Unlocking Potential. Th P3 06.

Liu, H., Sato, M., 2014. In situ measurement of pavement thickness and dielectric permittivity by GPR using an antenna array. NDT&E Int. 64, 65–71.

Lutz, P., Perroud, H., 2006. Phased-array transmitters for GPR surveys. J. Geophys. Eng. 3, 35–42.

Martins, S., Travassos, J., Sacchi, M., 2017. Interpolating GPR Data Using Anti-Alias Singular Spectrum Analysis (SSA) Method. Near Surface Geophysics. vol. 15 pp. 447–455.

Paglieroni, D., Chambers, D., Mast, J., Bond, S., Beer, N.R., 2015. Imaging modes for ground penetrating radar and their relation to detection performance. IEEE J. Selected Topics Appl. Earth Observ. Remote Sensing 8, 1132–1144.

Sato, M., Takayama, T., 2009. High range resolution directional borehole radar for 3-D fracture delineation. Proceedings of the IEEE International Geoscience and Remote Sensing Symposium. Vol. 1, pp. 132–135.

Sato, M., Yi, L., Iitsuka, Y., Zou, L., Takahashi, K., 2016. Optimization of antenna polarization of the multistatic GPR system Yakumo. 16th International Conference of Ground Penetrating Radar, p. 7572664.

Yilmaz, Ö., 2001. Seismic data analysis: processing, inversion and interpretation of seismic data. 2nd ed. Society Exploration Geophysicists, Tulsa, p. 2024.

Zhao, S., Al-Qadi, I., 2016. Development of an analytic approach utilizing the extended common midpoint method to estimate asphalt pavement thickness with 3-D ground-penetrating gradar. NDT&E Int. l78, 29–36.